




NUMERICAL INVESTIGATION OF TRANSONIC SHOCK WAVE CHARACTERISTICS ON SUPERCRITICAL AIRFOILS UNDER VARIOUS FLOW CONDITIONS

¹, * Mehmet Numan KAYA 


¹ Necmettin Erbakan University, Engineering Faculty, Mechanical Engineering Department, Konya, TÜRKİYE
mnkaya@erbakan.edu.tr

Highlights

- Shock behavior on RAE2822 was analyzed using the TSLAeroFoam CFD solver.
- Increasing angle of attack shifts the shock location closer to the leading edge.
- Higher Mach reduces pressure and lift; lift peaks at moderate angles of attack.
- Lift-to-drag ratio decreases with increasing Mach number and angle of attack.



NUMERICAL INVESTIGATION OF TRANSONIC SHOCK WAVE CHARACTERISTICS ON SUPERCRITICAL AIRFOILS UNDER VARIOUS FLOW CONDITIONS

1. * Mehmet Numan KAYA 

¹ Necmettin Erbakan University, Engineering Faculty, Mechanical Engineering Department, Konya, TÜRKİYE
¹ mnkaya@erbakan.edu.tr

(Received: 16.07.2025; Accepted in Revised Form: 12.08.2025)

ABSTRACT: This study numerically investigates transonic shock wave characteristics over supercritical airfoils using the OpenFOAM-based open-source solver TSLAeroFoam. The numerical setup is validated through comparison with benchmark transonic experimental results. A parametric study is conducted by varying the Mach number from 0.72 to 0.78 and the angle of attack from 3° to 7° to evaluate their effects on shock position, strength, shock–boundary layer interaction, and associated aerodynamic coefficients including lift, drag, and moment. Results indicate that increasing the angle of attack causes shock to move upstream toward the leading edge. Increasing the Mach number leads to a reduction in pressure on the lower surface and a corresponding decrease in lift coefficient. At a fixed angle of 3°, the lift coefficient dropped from nearly 0.71 to 0.60 as Mach number increased from 0.72 to 0.78. Additionally, the lift-to-drag ratio decreased significantly with both Mach number and angle of attack, dropping from approximately 37 to 16 at 3°, and from 12 to 8 at 7° for Mach numbers 0.72 and 0.78, respectively. The findings collectively demonstrate that both Mach number and angle of attack influence shock wave behavior and aerodynamic performance in transonic flows, with stronger effects observed at higher values of both parameters.

Keywords: CFD, OpenFOAM, RAE2822, Shock, Transonic, Wave

1. INTRODUCTION

Transonic flow, which occurs when the freestream Mach number is near one, presents a unique aerodynamic environment where both subsonic and supersonic regions coexist [1], [2]. A defining feature of transonic flow is the formation of shock waves, which can significantly alter pressure distributions, induce boundary-layer separation, and lead to unsteady aerodynamic forces. Understanding the structure and behavior of transonic shock waves, particularly in the context of shock-boundary layer interactions (SBLI) and unsteady flow phenomena such as shock buffet, is critical for improving aerodynamic performance and stability in engineering applications, including airfoil and wing design. Understanding the structure and dynamics of transonic shock waves is essential for improving aircraft design, flow control strategies, and numerical modeling approaches. The research in this area has largely focused on three interrelated themes: (1) shock-boundary layer interaction and flow separation [3], [4], [5], (2) unsteady shock oscillations and shock buffet [6], [7], and (3) numerical and experimental methods for analyzing transonic shock waves [8], [9].

Recent experimental and computational research has provided key insights into the dynamic nature of transonic shock waves and their interactions with boundary layers. Several studies have focused on the unsteady characteristics of shock oscillation and SBLI. Sartor et al. [10] investigated shock-wave/boundary-layer interactions in transonic channel flow over a bump, identifying distinct low- and medium-frequency unsteadiness linked to shock motion and shear-layer perturbations, respectively. Fourier analysis and global stability analysis revealed that these instabilities do not stem from unstable global modes but are instead likely due to external disturbances. Similarly, Bénard et al. [11] conducted experimental work on transonic SBLI over a bump and observed low-frequency shock behavior correlated with upstream-traveling pressure waves. Bruce et al. [12] examined forced unsteady shock wave behavior over transonic configurations, finding that at high frequencies the shock exhibits independent oscillatory

*Corresponding Author: Mehmet Numan KAYA, mnkaya@erbakan.edu.tr

disturbances. Chyu and Kuwahara [13] numerically investigated unsteady transonic flow over a pitching airfoil, emphasizing the role of shock-induced separation and turbulent boundary-layer interactions. Hu et al. [14] used computational fluid dynamics (CFD) with Detached Eddy Simulation (DES) to analyze shock buffet over a NACA0012 airfoil, demonstrating numerical agreement with experimental observations on transonic buffeting onset and aerodynamic load dynamics. Liu et al. [15] investigated transonic buffet behavior under ground effect using RANS-based CFD and found that the interaction between shock motion and vortex shedding produces distinct flow regimes depending on angle of attack, with significant influence from ground-induced Mach reflection and shock synchrony with vortex shedding. A significant challenge in transonic shock research is the prediction and mitigation of shock-induced separation and its effects on aerodynamic performance. Carter et al. [16] developed a coupled interaction model incorporating normal pressure gradients to better predict turbulent separation induced by transonic shocks. Vorobiev et al. [17] studied shock-separation interactions in transonic flow over a turret, proposing a low-dimensional model for phase-locked separation regions. Seifollahi and Jahangirian [18] investigated the use of active boundary-layer control techniques to reduce SBLI-induced drag via mass transfer. Matsuo et al. [19] further examined the impact of non-equilibrium condensation on shock strength and total pressure loss in a transonic internal flow, suggesting potential strategies for shock mitigation. Frede and Gatti [20] performed a parametric CFD study on active flow control via blowing and suction on the RAE2822 airfoil and found that suction on the suction side significantly reduced drag—up to 16%—in high-lift transonic conditions, whereas blowing increased drag due to nonlinear shock–boundary interactions. In addition to experimental and numerical studies, analytical and theoretical models continue to play a crucial role in transonic shock research. The study by Zhang et al. [21] has refined high-resolution computations of transonic shock behavior using advanced numerical schemes like WENO and RANS-LES methods to resolve complex flow interactions. More recently, Li et al. [22] examined how the number and configuration of bleed holes in a transonic stator affect shock–boundary layer interaction. Their results showed that increased porosity can reduce interaction length, but improper bleed patterns may increase wake losses. In a companion study, the same authors [23] demonstrated that combining suction on the suction surface and end-wall corner significantly suppresses both suction-side separation and corner stall. Similarly, Berizzi et al. [24] applied spanwise-travelling-wave wall forcing on the transonic RAE2822 airfoil, achieving shock delay of 7% chord length and nearly halving wave drag without significantly energizing the boundary layer. Liu et al. [25] numerically studied buffet on the OAT15A supercritical airfoil and showed that mesh resolution can be relaxed away from the shock/bubble zone without degrading buffet prediction accuracy.

Recent advances have deepened our understanding of transonic shock structures, their unsteady behavior, and the mechanisms driving shock–boundary layer interactions. However, despite substantial progress, there remains a need to further explore how shock wave characteristics evolve under varying flow conditions, especially in cases where both freestream Mach number and angle of attack vary concurrently. The aerodynamic response of supercritical airfoils becomes increasingly complex at higher Mach numbers and angles of attack, leading to nonlinear variations in shock position, intensity, and associated flow separation behavior. The interaction between these two parameters introduces a coupled effect on shock physics that is not yet fully resolved in existing studies. This study aims to address this gap by conducting a detailed numerical investigation into the aerodynamic effects of transonic shocks under multiple flow regimes, with a particular focus on how the interplay between Mach number and angle of attack influences shock location, strength, and airfoil performance.

2. MATERIAL AND METHODS

2.1. CFD Solver: TSLAeroFoam

In this work, the CFD method has been employed using TSLAeroFoam, an open-source solver developed within the OpenFOAM framework, to predict the flow physics. The solver discretizes the

continuity, momentum, and energy equations separately to obtain three linear systems [26], [27], [28], [29], [30].

$$\frac{\partial \rho}{\partial t} + \nabla \cdot (\mathbf{U}\rho) = 0 \quad (1)$$

$$\frac{\partial (\rho \mathbf{U})}{\partial t} + \nabla \cdot [\mathbf{U}(\rho \mathbf{U})] + \nabla p + \nabla \cdot \boldsymbol{\sigma} = 0 \quad (2)$$

$$\frac{\partial (\rho E)}{\partial t} + \nabla \cdot [\mathbf{U}(\rho E)] + \nabla \cdot (\mathbf{U}p) + \nabla \cdot (\boldsymbol{\sigma} \cdot \mathbf{U}) + \nabla \cdot \mathbf{j} = 0 \quad (3)$$

where ρ is density, \mathbf{U} is velocity, p is pressure, and E is total energy given by $E = e + |\mathbf{U}|^2/2$, with e representing the specific internal energy or enthalpy. The viscous stress tensor $\boldsymbol{\sigma}$ is defined as positive in compression:

$$\boldsymbol{\sigma} = -\mu \left[(\nabla \mathbf{U}) + (\nabla \mathbf{U})^T - \frac{2}{3} (\nabla \cdot \mathbf{U}) \mathbf{I} \right] \quad (4)$$

with dynamic viscosity μ , unit tensor \mathbf{I} , and diffusive heat flux \mathbf{j} with thermal conductivity k and temperature T :

$$\mathbf{j} = -k \nabla T \mathbf{s} \quad (5)$$

TSLAeroFoam is a steady-state, density-based compressible flow solver developed within the OpenFOAM-based NextFOAM framework. It employs the Lower-Upper Symmetric Gauss-Seidel (LUSGS) method for implicit time integration, enabling rapid convergence for steady computations. Tailored for aerospace flow simulations, the solver features Riemann-based boundary conditions and advanced near-wall modeling. Additionally, it adopts the thin shear layer approximation, which enhances computational efficiency for boundary layer-dominated transonic flows. Solver details are available in Ref. [31]. BaramFlow was used as the pre-processing interface for setting up the simulations. The source code and documentation of the NextFOAM framework, including TSLAeroFoam, are publicly available [32].

In this study, the convective fluxes are computed using the Roe-FDS (flux difference splitting) scheme with a VK-limited gradient reconstruction, while viscous fluxes are treated using the thin shear layer (TSL) approximation to improve efficiency in boundary layer-dominated transonic flows. A second-order upwind scheme is used for both convective and turbulence terms. Riemann-based boundary conditions are applied at the farfield, and no-slip adiabatic wall conditions are used on the airfoil surface. The solver includes advanced near-wall modeling, making it suitable for high-speed external aerodynamic simulations. A steady-state approach was employed for all simulations. Convergence was monitored via residuals, and each case was run for 10,000 iterations. By the end of the simulations, residuals of all primary flow variables had decreased below 10^{-5} , indicating satisfactory convergence.

2.2. Mesh Independency and Validation

To ensure the reliability and accuracy of the numerical results, a mesh independence study was conducted using three different grid resolutions: coarse, medium, and fine. Table 1 summarizes the number of cells and the corresponding aerodynamic coefficients for each mesh configuration, along with the experimental data used for validation. It is observed that the lift (C_L), drag (C_D), and moment (C_M) coefficients vary only slightly between the medium and fine meshes (nearly 0.15% for C_L and 0.26% for C_D , indicating mesh convergence. While the coarse mesh (49,858 cells) produces moderate deviations in aerodynamic coefficients, the medium (126,230 cells) and fine (193,402 cells) meshes yield nearly identical results. For instance, the lift coefficient increases from 0.7328 (coarse) to 0.7431 (medium) and 0.7442 (fine), whereas the drag and moment coefficients stay within a narrow range. The numerical results obtained using the medium mesh are sufficiently close to those of the fine mesh but require less computational cost.

The grid convergence index (GCI) between the medium and fine meshes was calculated to be less than 0.5%, confirming grid independence. Therefore, the medium mesh was selected for all subsequent simulations. The C-grid topology enables enhanced resolution at the leading and trailing edges and aligns the mesh with the expected flow direction, which helps reduce numerical dissipation. This structured approach also supports better boundary layer capture and numerical stability across a wide range of flow conditions. The mesh is refined near the airfoil surface to accurately resolve the boundary layer, with gradual coarsening toward the far field and additional refinement near the shock region to ensure better resolution of sharp gradients. The mesh structure corresponding to the selected medium-resolution grid is shown in Figure 1. The selected medium-resolution grid exhibits a maximum skewness, non-orthogonality and aspect ratio of approximately 0.80, 39.5° and 240, respectively which fall within acceptable limits for numerical stability. Moreover, the maximum y^+ value is below 3, ensuring sufficient near-wall resolution for accurate turbulence modeling. The $k-\omega$ SST turbulence model was employed in all simulations to accurately capture near-wall effects and shock–boundary layer interactions.

Table 1. Mesh independence study.

Type	Number of cells	C_L	C_D	C_M
coarse	49858	0.7328	0.0270	-0.0815
medium	126230	0.7431	0.02652	-0.0832
fine	193402	0.7442	0.02645	-0.0834
experimental	-	0.733	0.0188	-0.086

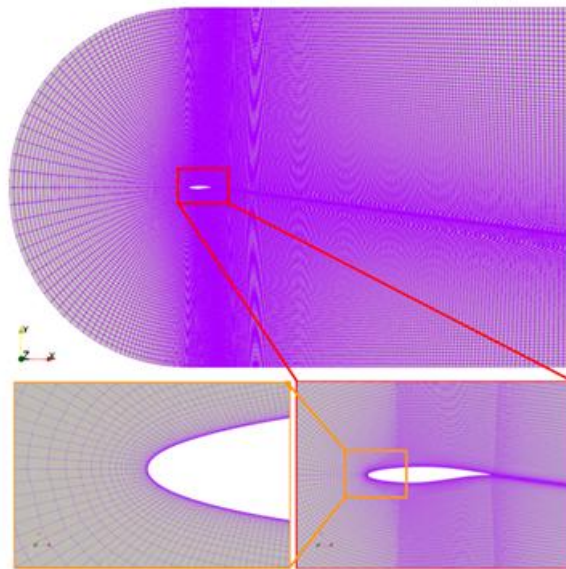


Figure 1. Some pictures from the selected medium-resolution grid.

The experimental data used for validation were obtained from the AGARD AR-138 report for the RAE2822 supercritical airfoil [33]. Specifically, Case 13A was selected, which corresponds to a Mach number of 0.739, Reynolds number of 2.7×10^6 , and an angle of attack of 3.19° . These conditions represent a typical transonic flow case with a pronounced shock, making it suitable for validation.

Figure 2 presents the surface pressure coefficient (C_p) distributions over the airfoil for all three mesh resolutions in comparison with the experimental data. All numerical predictions capture the general pressure trends and shock location reasonably well. However, the medium and fine meshes demonstrate slightly better agreement with the experimental data, particularly near the shock region around $x/c \approx 0.5$. The comparison confirms that the medium mesh provides a reliable balance between accuracy and computational efficiency.

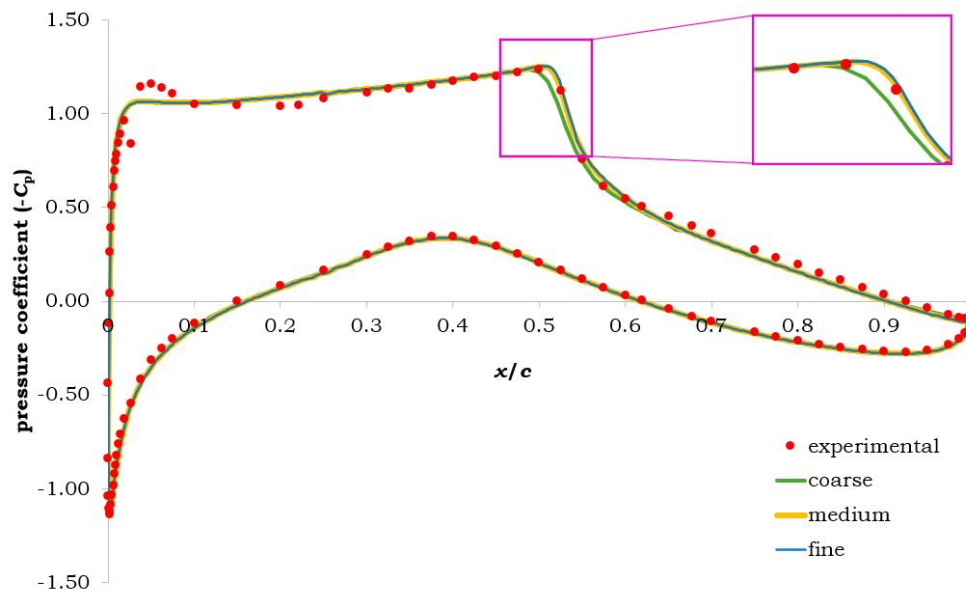


Figure 1. Comparison of surface pressure coefficients (C_p) for coarse, medium, and fine mesh resolutions, along with experimental data.

3. RESULTS AND DISCUSSION

This section presents the numerical results obtained from simulations under various Mach numbers and angles of attack, focusing on shock wave behavior and aerodynamic performance characteristics. Figure 3 illustrates the pressure coefficient (C_p) distributions on the airfoil surface for various Mach numbers and angles of attack. Each subfigure includes both a perspective view (top) and a plan view (bottom) of the pressure field. Across all Mach numbers, increasing the angle of attack from 4° to 6° results in a noticeable upstream movement of the shock wave on the upper surface. This is evidenced by the expansion of the low $-C_p$ (blue) region and the forward shift of high-gradient zones toward the leading edge. Overall, both Mach number and angle of attack significantly affect the shock wave's strength and position. The observed trends are consistent with typical transonic flow behavior over supercritical airfoils, supporting the capability of the solver to accurately capture key aerodynamic phenomena. Figure 4 shows the surface pressure coefficient distributions over the RAE2822 airfoil at four different Mach numbers ranging from 0.72 to 0.78 and for angles of attack between 3° and 7° . In all cases, increasing the angle of attack results in a stronger and more upstream-positioned shock wave, as indicated by the sudden change in C_p values on the suction surface. The shock location progressively moves toward the leading edge with increasing angle of attack. As the Mach number increases from 0.72 to 0.78, the shock wave shifts toward the trailing edge at low angles of attack. Additionally, a noticeable reduction in pressure is observed on the pressure side (lower surface), as seen by the upward shift of the C_p curves in this region. This indicates a weakening of the pressure difference between the suction and pressure sides. As a result, the overall pressure differential across the airfoil decreases, particularly at higher Mach numbers and angles of attack, which can affect lift generation and shock-boundary layer interaction. These trends confirm that both Mach number and angle of attack play a critical role in determining shock strength, position, and the aerodynamic performance of the airfoil under transonic conditions.

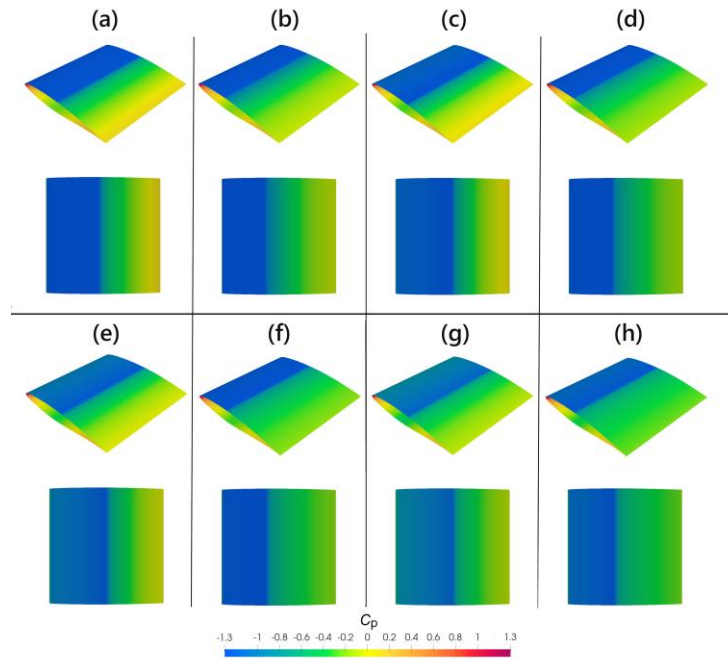


Figure 3. Pressure coefficient (C_p) contours on the airfoil surface at Mach numbers (a,b) 0.72, (c,d) 0.74 (e,f) 0.76 and (g,h) 0.78 for angles of attack of (a,c,e,g) 4° and (b,d,f,h) 6° .

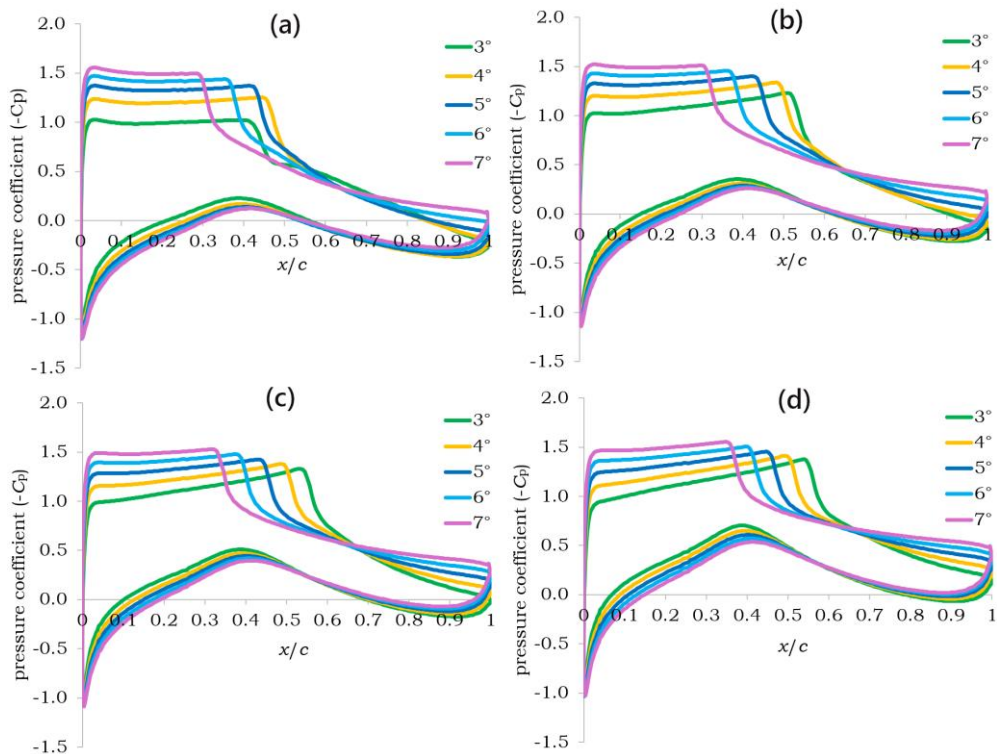


Figure 4. Pressure coefficient distributions at various Mach numbers: (a) $M=0.72$, (b) $M=0.74$, (c) $M=0.76$, (d) $M=0.78$ for angles of attack ranging from 3° to 7° .

Figure 5 displays the Mach number contours around the RAE2822 airfoil under various flow conditions, covering Mach numbers from 0.72 to 0.78 and angles of attack from 3° to 7° . Across all cases, the formation of a transonic shock on the suction surface is clearly observed. The shock induces abrupt changes in velocity, pressure, and density, which thicken the boundary layer downstream of the shock. Under stronger SBLI, this rapid deceleration may lead to adverse pressure gradients and reversed flow,

causing local flow separation on the suction surface. At lower Mach numbers and angles of attack, the flow remains largely attached, and the shock wave appears weak and positioned further downstream. As the Mach number increases, the shock becomes sharper and more prominent, with distinct red-to-green gradients indicating regions of rapid deceleration. This effect is especially noticeable at $M=0.78$ and 6° – 7° , where the shock wave strengthens and moves closer to the leading edge. Furthermore, the size and intensity of the supersonic region ahead of the shock increase with both Mach number and angle of attack. The downstream disturbances and shock reflections are also more apparent at higher conditions, indicating complex transonic wave dynamics.

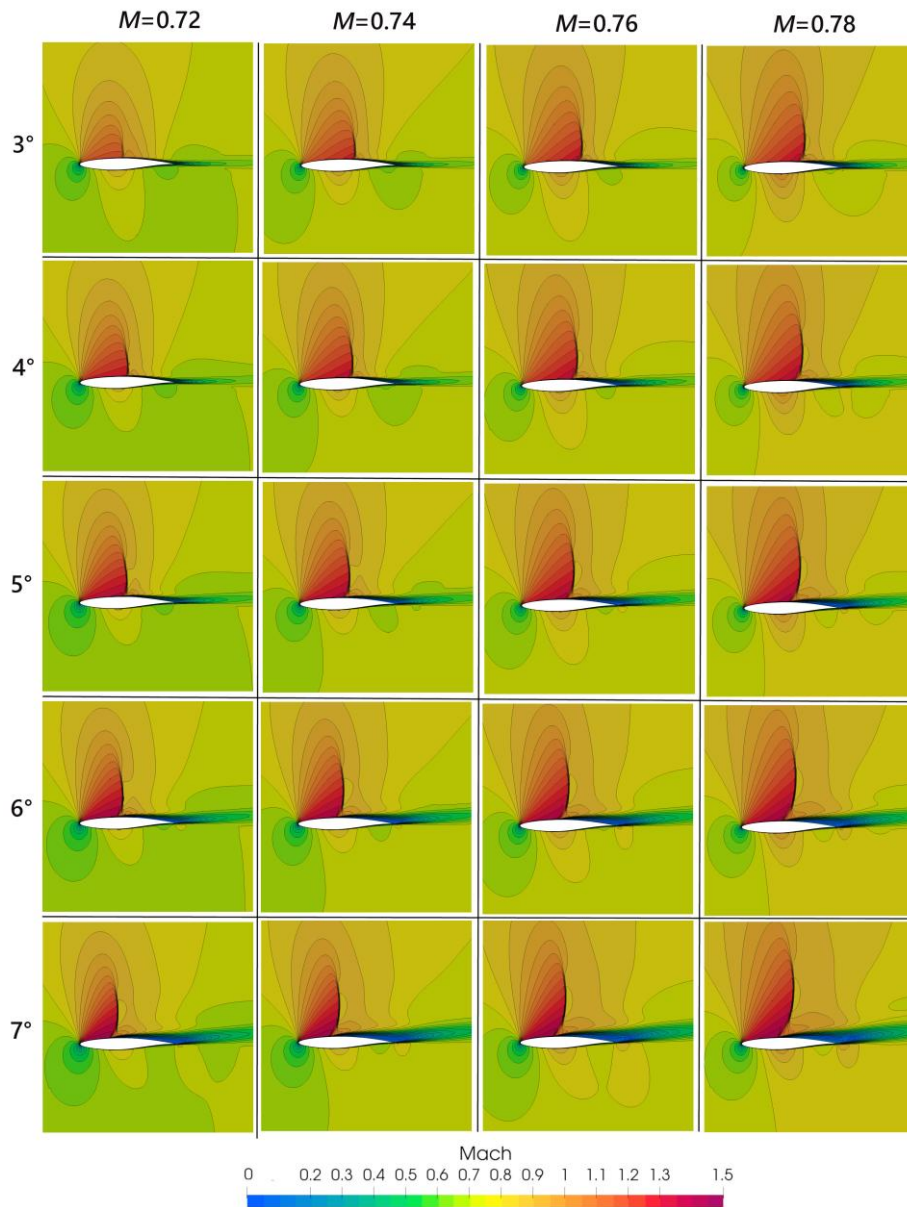


Figure 5. Mach number contours around the airfoil for Mach numbers 0.72, 0.74, 0.76, and 0.78, and angles of attack from 3° to 7° .

Figure 6 illustrates the variation of the lift coefficient (C_L) with angle of attack ranging from 3° to 7° for four Mach numbers: 0.72, 0.74, 0.76, and 0.78. For all Mach numbers, C_L increases with angle of attack as expected; however, a clear reduction in C_L is observed at higher Mach numbers for the same angle. At 3° , the lift coefficient decreases from approximately 0.706 at $M=0.72$ to 0.598 at $M=0.78$. A similar trend is

observed at 7°, where C_L values are approximately 0.927 for $M=0.72$ and 0.797 for $M=0.78$. This reduction reflects the increased compressibility effects and shock-induced losses at higher transonic speeds, which weaken the aerodynamic lifting capability of the airfoil.

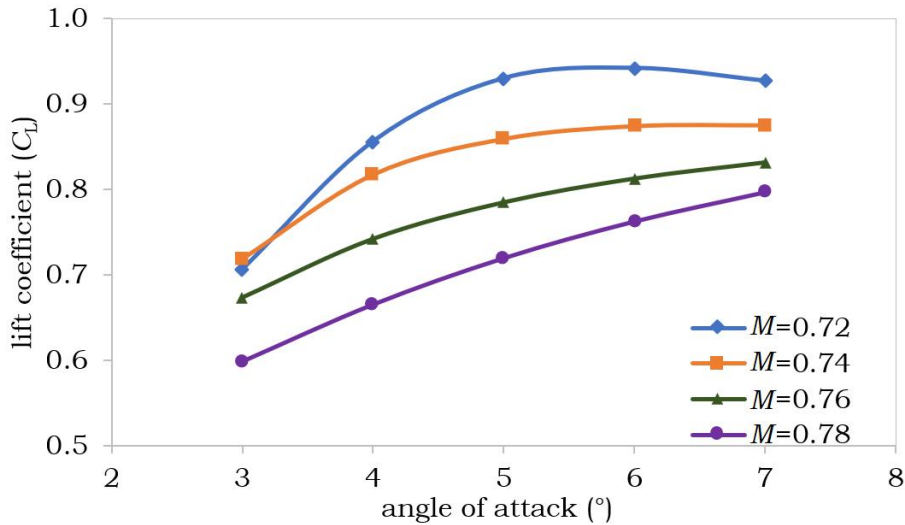


Figure 6. Variation of lift coefficient (C_L) with angle of attack (3°–7°) at Mach numbers ranging $M=0.72$ to 0.78.

Figure 7 shows the variation of the lift-to-drag ratio (C_L/C_D) with angle of attack for the same range of Mach numbers. As the angle of attack increases, C_L/C_D decreases significantly across all Mach numbers. At lower angles, the airfoil exhibits high aerodynamic efficiency, while at higher angles, drag increases more rapidly than lift, reducing the ratio. At 3°, the lift-to-drag ratio is approximately 37 for $M=0.72$ and 16 for $M=0.78$. By 7°, these values drop to around 12 and 8, respectively. This decline highlights the growing drag penalty and energy loss associated with stronger shock waves and boundary layer separation at higher Mach numbers and attack angles.

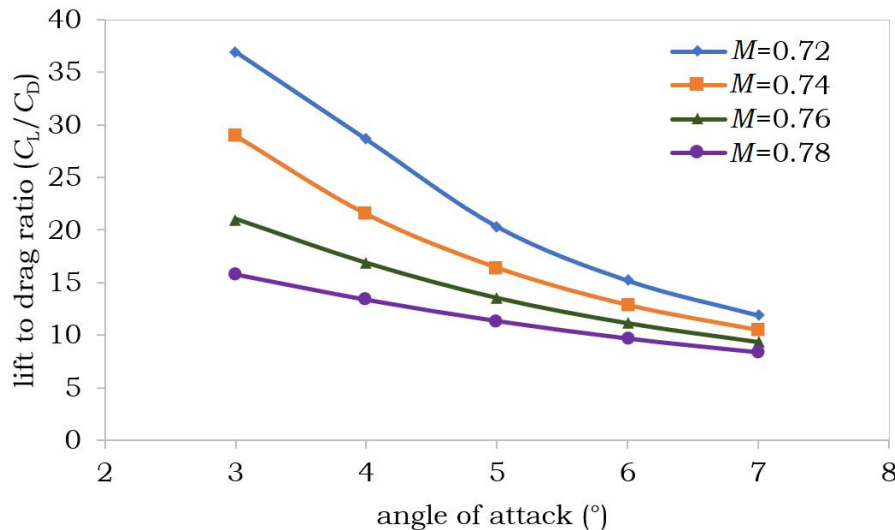


Figure 7. Variation of lift-to-drag ratio (C_L/C_D) with angle of attack (3°–7°) at Mach numbers ranging from $M=0.72$ to 0.78.

Table 2 presents the predicted aerodynamic coefficients for the RAE2822 supercritical airfoil across different Mach numbers and angles of attack (AoA). The results demonstrate clear trends in transonic flow behavior. The lift coefficient consistently decreases with increasing Mach number. At 3° angle of attack, C_L drops from 0.706 at $M=0.72$ to 0.598 at $M=0.78$, representing a 15.3% reduction due to strengthening shock waves and compressibility effects. The drag coefficient shows a substantial increase with Mach

number. At 3° , C_D doubles from 0.019 to 0.038 as Mach number increases from 0.72 to 0.78, primarily due to wave drag from shock formation. The moment coefficient becomes increasingly negative with higher Mach numbers, indicating center of pressure shifts. With respect to angle of attack, lift coefficient peaks around 6° before decreasing at higher angles, while drag keeps increasing across all Mach numbers.

Table 2. Aerodynamic coefficients predicted for different Mach numbers and angles of attack.

Mach →	0.72			0.74			0.76			0.78		
AoA ↓	C_L	C_D	C_M	C_L	C_D	C_M	C_L	C_D	C_M	C_L	C_D	C_M
3	0.706	0.019	-0.074	0.718	0.0248	-0.837	0.673	0.032	-0.091	0.598	0.038	0.0935
4	0.856	0.03	-0.073	0.817	0.038	-0.0821	0.742	0.044	-0.0866	0.665	0.0498	-0.0892
5	0.93	0.0458	-0.0706	0.859	0.0524	-0.0767	0.785	0.058	-0.0812	0.7195	0.0634	-0.0856
6	0.942	0.062	-0.065	0.874	0.068	-0.071	0.813	0.073	-0.077	0.7626	0.0786	-0.083
7	0.927	0.0782	-0.06	0.875	0.0837	-0.067	0.832	0.089	-0.074	0.797	0.0949	-0.0818

4. CONCLUSIONS

This study provided a comprehensive numerical assessment of transonic shock wave behavior over the RAE2822 supercritical airfoil using the open-source solver TSLAeroFoam. Key findings obtained under varying Mach numbers and angles of attack are summarized below:

- Increasing the angle of attack from 3° to 7° resulted in an upstream shift of the shock location toward the leading edge and intensified the shock–boundary layer interaction.
- A rise in Mach number led to a reduction in pressure on the pressure side of the airfoil, accompanied by a corresponding decrease in lift coefficient.
- The lift coefficient decreased with increasing Mach number at fixed angles of attack; for example, at 3° , C_L dropped from nearly 0.71 at $M=0.72$ to 0.60 at $M=0.78$.
- Increase in angle of attack generally led to increases in lift, drag and moment coefficients across all Mach numbers. However, the rate of increase diminished at higher angles, indicating a nonlinear aerodynamic response. Notably, at $M=0.72$, the lift coefficient reached its maximum value of nearly 0.94 at 6° , beyond which a slight decrease was observed.
- The lift-to-drag ratio also decreased with increasing angle of attack and Mach number. For example, at 3° , it dropped from approximately 37 at $M=0.72$ to 16 at $M=0.78$. As the angle of attack increased, the difference in C_L/C_D values between Mach numbers became less pronounced; at 7° , the ratio was about 12 at $M=0.72$ and 8 at $M=0.78$.

Overall, the results demonstrate that transonic flow characteristics are highly sensitive to both angle of attack and inflow Mach number. The observed trends provide insights into the complex aerodynamic behavior of supercritical airfoils operating in the transonic regime.

NOMENCLATURE

C_D	Drag coefficient
C_L	Lift coefficient
C_M	Moment coefficient
M	Mach number
Re	Reynolds number
x/c	Normalized chordwise position
AoA	Angle of attack ($^\circ$)
C_p	Pressure coefficient
SBLI	Shock–Boundary Layer Interaction

Declaration of Ethical Standards

The author declares to comply with all ethical guidelines, including authorship, citation, data reporting, and original research publication.

Declaration of Competing Interest

The author declares that he has no known competing financial interests or personal relationships that could have appeared to influence the work reported in this paper.

Funding / Acknowledgements

The author received no financial support for the research.

Data Availability

The data that support the findings of this study are available within the article.

REFERENCES

- [1] A. O. Yüksel, Ö. Kandemir, L. Uğur, Y. Ostovan, and E. Ayan, "Aerodynamic Buffet Onset Boundary Estimation of a Jet Trainer Aircraft," in *AIAA SCITECH 2023 Forum*, 2023, p. 2119.
- [2] O. Kocaaslan, K. M. Güleren, B. H. Saracoğlu, and T. Yasa, "Dönen Patlama Motorlarındaki Oluşan Dalga Yapısının Sayısal Olarak İncelenmesi," *Isı Bilimi ve Tekniği Dergisi*, vol. 44, no. 1, pp. 33–45, 2024.
- [3] F. Sartor, M. Clement, D. Sipp, and R. Bur, "Dynamics of a shock-induced separation in a transonic flow: a linearized approach," in *43rd AIAA Fluid Dynamics Conference*, 2013, p. 2735, doi: 10.2514/6.2013-2735.
- [4] X. Liu and L. Squire, "An investigation of shock/boundary-layer interactions on curved surfaces at transonic speeds," *Journal of Fluid Mechanics*, vol. 187, pp. 467–486, 1988, doi: 10.1017/S0022112088000527.
- [5] H. T. B. Ngoc and N. M. Hung, "Study of separation phenomenon in transonic flows produced by interaction between shock wave and boundary layer," *Vietnam Journal of Mechanics*, vol. 33, 2011, doi: 10.15625/0866-7136/33/3/210.
- [6] B. Lee, "Self-sustained shock oscillations on airfoils at transonic speeds," *Progress in Aerospace Sciences*, vol. 37, pp. 147–196, 2001, doi: 10.1016/S0376-0421(01)00003-3.
- [7] A. Alshabu and H. Olivier, "Unsteady Wave Phenomena on a Supercritical Airfoil," *AIAA Journal*, vol. 46, pp. 2066–2073, 2008, doi: 10.2514/1.35516.
- [8] M. Farahani and A. Jaber, "Experimental Investigation of Shock Waves Formation and Development Process in Transonic Flow," *Scientia Iranica*, vol. 24, pp. 2457–2465, 2017, doi: 10.24200/SCI.2017.4309.
- [9] H. Olivier and I. Klioutchnikov, "A numerical study of pressure/shock waves interactions in transonic airfoil flow using optimized WENO schemes," in *48th AIAA Aerospace Sciences Meeting Including the New Horizons Forum and Aerospace Exposition*, 2010, p. 924. doi: 10.2514/6.2010-924.
- [10] F. Sartor, C. Mettot, R. Bur, and D. Sipp, "Unsteadiness in transonic shock-wave/boundary-layer interactions: experimental investigation and global stability analysis," *Journal of Fluid Mechanics*, vol. 781, pp. 550–577, 2015, doi: 10.1017/jfm.2015.510.
- [11] E. Bénard, J.-C. Huang, and S. Raghunathan, "Experimental investigation of unsteadiness in transonic shock boundary layer interaction," in *45th AIAA Symposium of Applied Aerodynamics*, 2010, pp. 22–24.

- [12] P. Bruce, I. Coman, G. Holt, and J. Harvey, "Experimental investigations into transonic shock wave unsteadiness," in *49th AIAA Aerospace Sciences Meeting including the New Horizons Forum and Aerospace Exposition*, 2011. p. 1050.
- [13] W. Chyu and K. Kuwahara, "Computations of transonic flow over an oscillating airfoil with shock-induced separation," in *20th Aerospace Sciences Meeting*, 1982, p. 350.
- [14] Z. Hu, L. Zhu, X. Mo, and K. Shen, "Numerical study on transonic shock wave buffeting of airfoil," *Journal of Physics: Conference Series*, 2024, doi: 10.1088/1742-6596/2879/1/012032.
- [15] H. Liu, J. Sun, P. Li, D. Zheng, Y. Tao, and Z. Sun, "Investigation on transonic buffet of airfoil within ground effect," *Aerospace Science and Technology*, vol. 161, p. 110094, 2025.
- [16] J. Carter, D. Edwards, and M. Hafez, "Analysis of Transonic Shock Induced Separated Flow Including Normal Pressure Gradients.," 1983. doi: 10.2514/6.1985-371.
- [17] A. Vorobiev, S. Gordeyev, E. Jumper, S. Gogineni, A. Marruffo, and D. J. Wittich, "A Low-Dimensional Model of Shock-Wake Interaction Over Turrets at Transonic Speeds," in *45th AIAA Plasmadynamics and Lasers Conference*, 2014, p. 2357.
- [18] Z. S. Moghadam and A. Jahangirian, "Numerical Study of Active Shock Wave-Turbulent Boundary Layer Interaction Control for Transonic Aerodynamics," in *30th Congress of the International Council of the Aeronautical Sciences*, 2016.
- [19] S. Matsuo, K. Yokoo, J. Nagao, Y. Nishiyama, T. Setoguchi, H. D. Kim, and S. Yu, "Numerical Study on Transonic Flow with Local Occurrence of Non-Equilibrium Condensation," *Open Journal of Fluid Dynamics*, vol. 03, pp. 42–47, 2013, doi: 10.4236/ojfd.2013.32A007.
- [20] A. Frede and D. Gatti, "Investigation of blowing and suction for turbulent flow control on a transonic airfoil," *International Journal of Heat and Fluid Flow*, vol. 113, p. 109769, 2025.
- [21] L. Zhang, S. Ma, F. Liu, and X. Cui, "Numerical Investigation for Separation Characteristics of Transonic Shock Oscillations Based on Parallel Computing," *Journal of Physics: Conference Series*, vol. 1631, 2020, doi: 10.1088/1742-6596/1631/1/012152.
- [22] B. Li, X. Zhou, L. Luo, and W. Du, "Effects of number of bleed holes on shock-wave/boundary-layer interactions in a transonic compressor stator," *Journal of Thermal Science*, vol. 33, no. 2, pp. 611–624, 2024.
- [23] B. Li, G. Mu, L. Luo, W. Du, and X. Zhou, "Effect of combined boundary layer suction on the separation control in a highly loaded transonic compressor cascade," *Proceedings of the Institution of Mechanical Engineers, Part A: Journal of Power and Energy*, vol. 238, no. 2, pp. 217–231, 2024.
- [24] N. Berizzi, D. Gatti, G. Soldati, S. Pirozzoli, and M. Quadrio, "Aerodynamic performance of a transonic airfoil with spanwise forcing," *Journal of Fluid Mechanics*, vol. 1010, p. A18, 2025.
- [25] T. Liu, X. Chen, Z. Tian, and J. Li, "Prediction of transonic shock buffet over supercritical airfoil OAT15A based on zonal detached-eddy simulation," *Applied Sciences*, vol. 14, no. 21, p. 9628, 2024.
- [26] O. V. Özdemir, H. Amiri, and U. C. Küçük, "RAE M2129 S-Shaped Air Intake CFD Analysis Using OpenFOAM," in *2023 10th International Conference on Recent Advances in Air and Space Technologies (RAST)*, 2023, pp. 1–6.
- [27] M. N. Kaya, S. Satcunanathan, M. Meinke, and W. Schröder, "Leading-Edge Noise Mitigation on a Rod–Airfoil Configuration Using Regular and Irregular Leading-Edge Serrations," *Applied Sciences*, vol. 15, no. 14, p. 7822, 2025.
- [28] E. Canli, H. Kucuksariyildiz, and K. Carman, "Impact assessment of new generation high-speed agricultural tractor aerodynamics on transportation fuel consumption and related phenomena," *Environmental Science and Pollution Research*, vol. 30, no. 3, pp. 6658–6680, 2023.
- [29] M. Manolesos, Y. Celik, H. Ramsay, R. Karande, B. Wood, I. Dinwoodie, I. Masters, M. Harrold and G. Papadakis, "Performance improvement of a Vestas V52 850kW wind turbine by retrofitting passive flow control devices," in *Journal of Physics: Conference Series*, vol. 2767, no. 2, 2024.
- [30] M. E. Tolu, O. Babayiğit, and D. N. Özen, "Investigation of the effects of rib application on cooling in a turbine blade," *Konya Journal of Engineering Sciences*, vol. 13, no. 1, pp. 11–24, 2025.

- [31] K. K. You, J. H. Ha, and S. C. Lee, "An Automated Aerodynamic Analysis System in Missile Based on Open-Source Software," *International Journal of Aeronautical and Space Sciences*, vol. 24, no. 3, pp. 592–605, 2023.
- [32] NextFOAM, "NextFOAM CFD Framework", 2025. [Online]. Available: <https://github.com/nextfoam/nextfoam-cfd>. [Accessed: Jun. 6, 2025].
- [33] P. H. Cook, M. C. P. Firmin, and M. A. McDonald, *Aerofoil RAE 2822: pressure distributions, and boundary layer and wake measurements*. AGARD Advisory Report AR-138, 1979.